Ocean Modelling 47 (2012) 55–64

Contents lists available at SciVerse ScienceDirect

Ocean Modelling

journal homepage: www.elsevier.com/locate/ocemod

Coupling of a discontinuous Galerkin finite element marine model with a finite difference turbulence closure model

Tuomas Kärnä [a,b,*], Vincent Legat [a,b], Eric Deleersnijder [a,c], Hans Burchard [d]

[a] Université catholique de Louvain, Institute of Mechanics, Materials and Civil Engineering (IMMC), Avenue Georges Lemaître 4, B-1348 Louvain-la-Neuve, Belgium
[b] Université catholique de Louvain, G. Lemaître Centre for Earth and Climate Research (TECLIM), Chemin du Cyclotron 2, B-1348 Louvain-la-Neuve, Belgium
[c] Université catholique de Louvain, Earth and Life Institute (ELI), G. Lemaître Centre for Earth and Climate Research (TECLIM), Chemin du Cyclotron 2, B-1348 Louvain-la-Neuve, Belgium
[d] Leibniz Institute for Baltic Sea Research, Seestraße 15, D-18119 Warnemünde, Germany

ARTICLE INFO

Article history:
Received 31 July 2011
Received in revised form 6 January 2012
Accepted 10 January 2012
Available online 25 January 2012

Keywords:
Finite element method
Discontinuous Galerkin
Finite difference method
Turbulence closure
Coupling

ABSTRACT

This paper describes an online coupling between a 3D discontinuous Galerkin finite element marine model and a 1D vertical turbulence closure model based on finite differences. The coupling exploits the topology of the 3D mesh, that is formed by stacking layers of prisms in the vertical direction. A robust mapping between the finite difference grid and the finite element function space is designed, taking into account the discontinuities in the latter. The coupling is tested with two horizontally homogeneous flows and an idealised 3D estuary simulation. The results are in good agreement with those obtained with a finite difference model using the same turbulence closure, indicating that the coupling does not deteriorate the performance of the turbulence model.

1. Introduction

Three-dimensional marine models usually rely on Fourier–Fick parametrisations to represent vertical fluxes due to unresolved fluctuations. The relevant eddy coefficients are obtained by means of turbulence closure schemes. While in some applications simple formulations, such as algebraic expressions of eddy viscosity/diffusivity, can be sufficient, in general more sophisticated models are needed to account for the time–space evolution of the turbulent fluxes.

Most popular high-level turbulence models consist of two partial differential equations, one for the turbulent kinetic energy (TKE) and another one for an accompanying variable that determines the relevant length scale. Such turbulence closures include the widely used model by Mellor and Yamada (1982) (level 2.5), k–ε (Rodi, 1987), k–ω (Wilcox, 1988; Umlauf et al., 2003) and a recent generic length scale (GLS) model by Umlauf and Burchard (2003). Choosing a turbulence model is not trivial as it may have a high impact on mixing and circulation (Ruddick et al., 1995; Luyten et al., 1996; Burchard et al., 1998; Burchard, 2002; Wijesekera et al., 2003; Warner et al., 2005).

GOTM[1] (General Ocean Turbulence Model, Burchard et al., 1999) is a library that implements a generic turbulence closure model, in which all the above models can be easily obtained by changing parameters. GOTM is based on a finite difference (FD) formulation on a 1D vertical grid. It has been extensively tested and validated in numerous studies. Offering the flexibility to easily switch from one closure to another, GOTM is an advantageous tool for marine modelling.

GOTM has been coupled to many structured grid FD or finite volume (FV) models, including GETM (General Estuarine Transport Model, Burchard and Bolding, 2002) and MOM (Modular Ocean Model, Griffies, 2010). Enstad et al. (2008) studied CO_2 transport in a lake using GOTM with MITgcm (Massachusetts Institute of Technology general circulation model). Rygg et al. (2009) used GOTM with both MITgcm and BOM (Bergen Ocean Model) in a similar study. Also POLCOMS (Proudman Oceanographic Laboratory Coastal Ocean Modelling System) has been coupled to GOTM to simulate tidal mixing and stratification in the Northwest European Continental shelf (Holt and Umlauf, 2008). Among unstructured grid models GOTM has been coupled to FVCOM (Finite Volume Coastal Ocean Model, Chen et al., 2006; Tian and Chen, 2006).

Creating an interface between a 1D FD turbulence model and a FD/FV circulation model is fairly straightforward given the

* Corresponding author at: Université catholique de Louvain, Institute of Mechanics, Materials and Civil Engineering (IMMC), Avenue Georges Lemaître 4, B-1348 Louvain-la-Neuve, Belgium. Tel.: +32 10478031; fax: +32 10472180.
E-mail address: tuomas.karna@uclouvain.be (T. Kärnä).

[1] www.gotm.net

1463-5003/$ - see front matter © 2012 Elsevier Ltd. All rights reserved.
doi:10.1016/j.ocemod.2012.01.001

similarities in the grid and the mathematical representation of the fields. The purpose of this paper is to investigate the possibility of coupling GOTM to a discontinuous Galerkin (DG) finite element (FE) marine model. Such a coupling is feasible as long as the unstructured FE grid is vertically aligned, such as in the case of the commonly used prismatic mesh. Equipotential z-grids, terrain following σ-grids and their generalisations are equally applicable. However, due to the DG formulation, exchanging data becomes more complicated because fields are represented as a piecewise discontinuous polynomial on the domain, in contrast to a set of discrete values in FD.

FE marine models have been equipped with various turbulence closure models. FEOM (Finite Element Ocean Model, Wang, 2007) uses a Richardson number dependent Pacanowski and Philander (1981) parametrisation. More sophisticated Mellor–Yamada level 2.5 closure has been implemented in a 1D water column model (Hanert et al., 2006, 2007; Blaise and Deleersnijder, 2008) and a full 3D model in Blaise et al. (2007). The SELFE (Semi-implicit Eulerian–Lagrangian Finite Element) model implements the GLS turbulence closure (Zhang and Baptista, 2008). However, all these FE models are based on *continuous Galerkin* (CG) formulation, i.e. the basis functions are continuous between elements. White et al. (2008) present a FE model that features discontinuous fields in the vertical direction, but rely on a simple parabolic parametrisation of eddy viscosity. Therefore, to our knowledge, sophisticated turbulence models in *discontinuous Galerkin* framework have not been dealt with so far.

As established models are nowadays mainly based on structured meshes and FD formulation, while unstructured mesh models are still emerging and mostly applied to regional studies, it is clear that there is a need to develop interfaces between the two model classes. This paper is a contribution to such a coupling. The aim is to take the best of both worlds, i.e. combining novel FE ocean model developments with an established FD turbulence library.

The article is organised as follows. The governing equations are presented in Section 2. Section 3 presents the numerical models: the 3D model and its DG-FE function space are briefly presented in Section 3.1, while the spatial discretisation and the interface of GOTM are outlined in Section 3.2. The coupling strategy is presented in Section 4. Numerical tests and concluding remarks are presented in Sections 5 and 6, respectively.

2. Governing equations

2.1. Shallow water equations

The three-dimensional flow is simulated by the shallow water equations in Cartesian coordinates $[x,y,z]^T$, the vertical coordinate z increasing upwards. The horizontal momentum equation reads

$$\frac{\partial \boldsymbol{u}}{\partial t} + \nabla_h \cdot (\boldsymbol{u}\boldsymbol{u}) + \frac{\partial (w\boldsymbol{u})}{\partial z} + f\boldsymbol{e}_z \wedge \boldsymbol{u}_{3D} + g\nabla_h r + g\nabla_h \eta = \frac{\partial}{\partial z}\left((\nu_0 + \nu)\frac{\partial \boldsymbol{u}}{\partial z}\right), \tag{1}$$

and the continuity equation is

$$\nabla_h \cdot \boldsymbol{u} + \frac{\partial w}{\partial z} = 0. \tag{2}$$

Integrating (2) over the vertical, and taking into account the impermeability of the surface and the bottom, leads to the free surface equation

$$\frac{\partial \eta}{\partial t} + \nabla_h \cdot \int_{-h}^{\eta} \boldsymbol{u} dz = 0. \tag{3}$$

Here, u, v and w are the velocity components in the Cartesian coordinates, $\boldsymbol{u}_{3D} = [u,v,w]^T$, $\boldsymbol{u} = [u,v]^T$ denotes the horizontal velocity, ∇_h is the horizontal gradient operator, f is the Coriolis parameter, g is the gravitational acceleration, η is the free surface elevation, h is the water column depth at rest, ν_0 and ν are the molecular and (vertical) eddy viscosity, respectively. The vertical unit vector is denoted by $\boldsymbol{e}_z$. The gravity is always orthogonal to the horizontal plane and level $z = 0$ corresponds to the water elevation at rest ($\eta = 0$).

The vertical velocity is computed diagnostically from the continuity constraint (2). The density is obtained from the equation of state (Jackett et al., 2006) using the potential temperature T, the salinity S and the hydrostatic pressure p

$$\rho = \rho_0 + \rho'(T,S,p), \tag{4}$$

where ρ_0 and ρ' are the constant reference density and the density deviation, respectively.

The baroclinic head is given by

$$r = \frac{1}{\rho_0}\int_z^{\eta} \rho' dz'. \tag{5}$$

Furthermore, the transport equations for T and S are solved (μ denotes the vertical eddy diffusivity, $\mu_{T,0}$ and $\mu_{S,0}$ are the corresponding molecular diffusivities):

$$\frac{\partial T}{\partial t} + \nabla_h \cdot (\boldsymbol{u}T) + \frac{\partial wT}{\partial z} = \frac{\partial}{\partial z}\left((\mu_{T,0} + \mu)\frac{\partial T}{\partial z}\right), \tag{6}$$

$$\frac{\partial S}{\partial t} + \nabla_h \cdot (\boldsymbol{u}S) + \frac{\partial wS}{\partial z} = \frac{\partial}{\partial z}\left((\mu_{S,0} + \mu)\frac{\partial S}{\partial z}\right). \tag{7}$$

For brevity, the horizontal viscosity and diffusivity terms in the above equations have been omitted as they are irrelevant for the current discussion.

In this paper the molecular viscosity/diffusivity constants are taken to be $\nu_0 = 1.3 \times 10^{-6}\ \mathrm{m^2\ s^{-1}}$, $\mu_{T,0} = 1.4 \times 10^{-7}\ \mathrm{m^2\ s^{-1}}$, $\mu_{S,0} = 1.1 \times 10^{-9}\ \mathrm{m^2\ s^{-1}}$. To close the set of equations, the vertical eddy viscosity ν and diffusivity μ need to be solved for.

2.2. Turbulence closure models

Eddy viscosity and eddy diffusivity are calculated as proportional to a turbulence velocity scale $k^{1/2}$ (where k is the turbulent kinetic energy, TKE, per unit mass) and an integral turbulent length scale l:

$$\nu = c_\nu k^{1/2} l, \quad \mu = c_\mu k^{1/2} l. \tag{8}$$

The dimensionless proportionality factors, c_ν and c_μ, are stability functions, depending on non-dimensional shear and buoyancy frequency squared,

$$\alpha_M = \frac{M^2 l^2}{k}, \quad \alpha_N = \frac{N^2 l^2}{k}, \tag{9}$$

respectively. Here M^2 stands for the vertical shear frequency squared and N^2 is the vertical buoyancy (Brunt–Väisälä) frequency squared, defined as

$$M^2 = \left(\frac{\partial u}{\partial z}\right)^2 + \left(\frac{\partial v}{\partial z}\right)^2, \tag{10}$$

$$N^2 = -\frac{g}{\rho_0}\frac{\partial \rho}{\partial z}. \tag{11}$$

Second moment turbulence closure models are derived from the Reynolds Averaged Navier–Stokes (RANS) equations, leading to transport equations for the Reynold stresses and turbulent tracer fluxes (Burchard, 2002). These equations are then closed by assuming a local equilibrium and finding suitable second moment parametrisations for the unknown third moments. Classical second-moment closures are those by Mellor and Yamada (1982) and Canuto et al. (2001).

In the present framework, k and l are calculated by means of two budget equations. The k-equation is derived form the Navier–Stokes equations under the assumption of vertical shear layers and the turbulent TKE transport being down-gradient. The resulting transport equation reads as

$$\frac{\partial k}{\partial t}+\nabla_h\cdot(\boldsymbol{u}k)+\frac{\partial(wk)}{\partial z}=\frac{\partial}{\partial z}\left(\frac{\nu}{\sigma_k}\frac{\partial k}{\partial z}\right)+P+B-\varepsilon, \tag{12}$$

with the constant turbulent Schmidt number, σ_k, the shear and buoyancy production terms

$$P=\nu M^2,\quad B=-\mu N^2, \tag{13}$$

respectively, and the viscous dissipation rate per unit mass, ε. The latter can be calculated from k and l by means of

$$\varepsilon=\left(c_\mu^0\right)^3\frac{k^{3/2}}{l}, \tag{14}$$

with the empirical dimensionless parameter c_μ^0.

The internal turbulent length scale l is calculated by the means of the generic two-equation turbulence closure model developed by Umlauf and Burchard (2003). It introduces another transport equation for the generic quantity

$$\Psi=\left(c_\mu^0\right)^p k^m l^n, \tag{15}$$

with real numbers p, m and n.

Clearly, for $p=3$, $m=3/2$ and $n=-1$, $\Psi=\varepsilon$ is obtained. Along with the k-equation, this set of parameters results in the well-known k–ε model (Rodi, 1987). Other well known quantities for which budget equations have been derived are the turbulence frequency $\omega=\left(c_\mu^0\right)^{-1}k^{1/2}l^{-1}$ (Wilcox, 1988; Umlauf et al., 2003) and kl (Mellor and Yamada, 1982). The transport equation for Ψ as derived by Umlauf and Burchard (2003) reads

$$\frac{\partial\Psi}{\partial t}+\nabla_h\cdot(\boldsymbol{u}\Psi)+\frac{\partial(w\Psi)}{\partial z}=\frac{\partial}{\partial z}\left(\frac{\nu}{\sigma_\Psi}\frac{\partial\Psi}{\partial z}\right)+\frac{\Psi}{k}(c_{\psi1}P+c_{\psi3}B-c_{\psi2}\varepsilon), \tag{16}$$

with the empirical parameters $c_{\psi1}$,$c_{\psi2}$, and $c_{\psi3}$, and the turbulent Schmidt number σ_Ψ. The transport Eq. (16) has been derived by combining (12) with the highly empirical ε-equation (Rodi, 1987). However, the empirical parameters have a clear physical meaning, as discussed by Umlauf and Burchard (2003). The role of $c_{\psi3}$ for properly adjusting the balance between increased mixing due to shear and decreased mixing due to stable stratification has been highlighted by Burchard and Baumert (1995) and Umlauf and Burchard (2005) by analysing conditions for steady state solutions of (12) and (16) for homogeneous shear layers (i.e. zero gradients of k and Ψ):

$$P+B=\varepsilon,\quad c_{\psi1}P+c_{\psi3}B=c_{\psi2}\varepsilon, \tag{17}$$

which implies

$$R_i^{st}=\frac{c_{\psi1}-c_{\psi2}}{c_{\psi3}-c_{\psi2}}\cdot\frac{c_\mu(R_i^{st})}{c_\nu(R_i^{st})} \tag{18}$$

and

$$\Gamma^{st}=\frac{c_{\psi1}-c_{\psi2}}{c_{\psi3}-c_{\psi1}}, \tag{19}$$

with the steady state gradient Richardson number, $R_i^{st}=N^2/M^2$ and the steady state mixing efficiency, $\Gamma^{st}=-B/\varepsilon$, where M and N are shear and buoyancy frequency fulfilling (17). It should be noted that the stability functions c_ν and c_μ are functions of R_i^{st} only for turbulence equilibrium $P+B=\varepsilon$. By means of (18), $c_{\psi3}$ can be calculated as function of R_i^{st} which is expected to be $R_i^{st}=0.25$ (Shih et al., 2000). Burchard and Hetland (2010) showed that when calculating $c_{\psi3}$ using the stability functions developed by Cheng et al. (2002), a steady-state mixing efficiency of $\Gamma^{st}=0.22$ is obtained by means of (19), a value close to the estimate by Osborn (1980).

The most stable boundary conditions for k and l have proved to be Neumann conditions, which are generally derived from the law of the wall and depend on the surface friction velocity u_*^s and the bottom friction velocity u_*^b, unless surface wave breaking effects are considered (Umlauf and Burchard, 2005).

3. Numerical models

3.1. 3D Finite element ocean model

In this work we use the Second-generation Louvain-la-Neuve Ice-ocean Model (SLIM[2]). SLIM is based on the discontinuous Galerkin finite element method, and consists of 1D, 2D and 3D shallow water models.

SLIM 2D has been applied to various studies. Modelling the flow in the entire Great Barrier Reef, Australia, is presented in Lambrechts et al. (2008) with validation against measurement data. Coupled 2D-1D model has been applied to modelling the Scheldt river, estuary and adjacent coastal zone, where the tidal water elevation is simulated with good accuracy across the multi-scale domain (de Brye et al., 2010).

White et al. (2008) present an early barotropic version of SLIM 3D model with semi-discontinuous function space. Full DG discretisation of the 3D baroclinic equations is presented in Blaise et al. (2010) and an implicit–explicit Runge–Kutta time integration method in Comblen et al. (2010). In contrast to the references above, the 3D simulations in this paper are conducted using a simple explicit time integration scheme (third order Adams–Bashforth), except for vertical diffusion which is treated semi-implicitly.

3.1.1. Spatial discretisation of SLIM

For solving boundary value problems with the finite element method, the domain is divided into a finite number of elements. By means of the elements, a discrete function space, spanned by a set of basis functions, is defined. A FE solution belongs to this function space and approximates the exact solution of the boundary value problem in the sense of the L_2 norm. Consequently, a FE solution is a function defined in the entire domain, instead of a set of discrete values as in FD. Usually Lagrangian basis functions are used, which implies that the nodal values are interpolated inside the elements.

In SLIM the 3D mesh is made up of prismatic elements (see leftmost panel in Fig. 1). Each element is a triangular prism of order o, that is formed as a product of a oth order triangle in horizontal and oth order linear element in vertical. As such, the solution is a piecewise polynomial of degree o in both horizontal and vertical directions. Due to the discontinuous Galerkin (DG) formulation, the solution is discontinuous at the element interfaces. The same spatial discretisation is used for all fields.

Assuming that there are n^E elements in the mesh, an element is identified by an integer $e=1,\ldots,n^E$. Each element e contains n_e^N nodes, and consequently a node is identified by a pair of integers, (e,ξ), $\xi=1,\ldots,n_e^N$. The set of all nodes (e,ξ) is denoted by $\mathcal{D}$. The nodal values of a field u are denoted by $u_{(e,\xi)}$. Denoting the ξth basis function of the element e as $\psi_{(e,\xi)}$, a field is expressed as $u_h=\sum_{(e,\xi)\in\mathcal{D}}u_{(e,\xi)}\psi_{(e,\xi)}(x,y,z)$, which is a discontinuous piecewise polynomial of degree o. In this work we are concentrating on first order elements, i.e. $o=1$.

[2] www.climate.be/slim

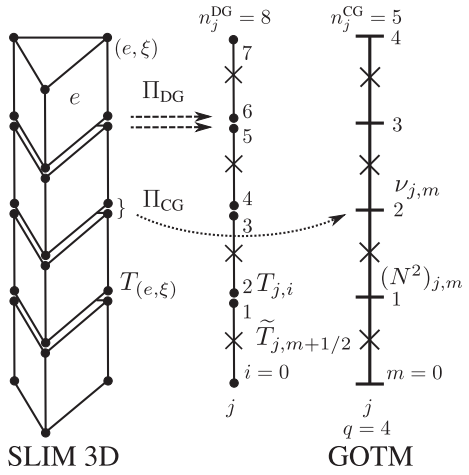

Fig. 1. Schematic illustration of the coupling. The operator Π_{DG} maps 3D nodes (e,ξ) to DG nodes in the corresponding 1D vertical mesh. Π_{CG} maps 3D nodes to cell interfaces (j,m) in GOTM. For illustration purposes, the discontinuities of the SLIM 3D mesh has been exaggerated; in reality there is no gap between the elements.

3.2. GOTM turbulence closure model

GOTM solves the Eqs. (12) and (16), except for the advection terms that must be implemented in the 3D circulation model. GOTM uses a 1D vertical staggered grid extending from the bed to the fluctuating free surface, divided into q cells (see the rightmost panel in Fig. 1). Internally, the mean flow variables are defined in the cell centres (crosses in Fig. 1), while the turbulent variables are defined at cell interfaces. Thus the mean flow variables are denoted by $u_{m+1/2}, m = 0,\ldots,q-1$ while the turbulent quantities read $v_m, m = 0,\ldots,q$.

3.2.1. GOTM interface

The variables required at runtime by GOTM are listed in Table 1. The user must provide the input variables at each time step. The output variables evolve in time and are updated by GOTM. If a single GOTM instance is used for computing several 1D segments, the output variables of the previous iteration must be provided. Consequently, one must store the arrays $v_{j,m}$, $\mu_{j,m}$, $k_{j,m}$, $\varepsilon_{j,m}$ for each vertical segment j.

4. Coupling strategy

4.1. Mapping nodes between 3D and 1D

In order to couple a 3D model with the 1D turbulence model, one needs to define vertical segments in the discontinuous 3D mesh, and build a mapping between the corresponding nodes.

In the simplest form, a 1D vertical array is built for each (discontinuous) node in the triangular surface mesh. Then there exists a bijective mapping Π_{DG} that maps each 3D node to a position i in a vertical array j. Using the nodal values of a field u in the 3D mesh, $u_{(e,\xi)}$, the values at the 1D array are denoted $u_{j,i} = \Pi_{DG} u_{(e,\xi)}, i = 0, \ldots, n_j^{DG} - 1$.

The 1D array defined above is discontinuous in the vertical. To account for the fact that the 1D FD grid has only continuous (unique) values at the cell interfaces, another mapping Π_{CG} is needed. Unlike above, Π_{CG} ignores the discontinuities in vertical, and hence it is no longer a bijection. Π_{CG} is used to fetch GOTM generated data back to the 3D fields, denoted by $v_{(e,\xi)} = \Pi_{CG} v_{j,m}$. Consequently the field $v_{(e,\xi)}$ is continuous in the vertical direction.

The mappings Π_{DG} and Π_{CG} are illustrated in Fig. 1. For first order elements it holds $n_j^{CG} = n_j^{DG}/2 + 1$.

Table 1
Input and output variables in the GOTM interface with q cells.

User provided input		m
H	Total depth	
u_*^s	Surface friction velocity	
u_*^b	Bottom friction velocity	
z_0^s	Surface roughness length	
z_0^b	Bottom roughness length	
$d_{m+1/2}$	Cell height	$0,\ldots,q-1$
N_m	Buoyancy frequency	$1,\ldots,q-1$
M_m	Vert. shear frequency	$1,\ldots,q-1$
Output		m
ν_m	Turbulent vert. viscosity	$0,\ldots,q$
μ_m	Turbulent vert. diffusivity	$0,\ldots,q$
k_m	Turbulence kinetic energy	$0,\ldots,q$
ε_m	TKE dissipation rate	$0,\ldots,q$

Alternatively, the 1D vertical arrays can be located at the centroids of the surface triangles. In this case there exists only a single 1D array for each column of prisms. In order to fetch data from the 3D mesh to such an array, the FE basis functions are evaluated at the DG points corresponding to the triangle centroid, which can be seen as a generalisation of the map Π_{DG}. To map turbulent quantities back to the 3D mesh, the 1D values are copied to the entire column of prisms, i.e. the values are constant in the horizontal, and linear continuous in the vertical direction. The 3D field is further smoothed in horizontal direction by taking a nodal average weighted by the volume associated to each node. This approach provides horizontal filtering on the input data, which improves the stability of the turbulence closure model in the presence of strong horizontal gradients.

4.2. Computing M and N

The key input parameters for GOTM are the vertical shear frequency M and buoyancy frequency N, defined in (10) and (11).

The buoyancy frequency requires the computation of the vertical gradient of the potential density, which is obtained by differentiating the equation of state at a constant pressure

$$\frac{\partial \rho}{\partial z} = A(T,S,p)\frac{\partial T}{\partial z} + B(T,S,p)\frac{\partial S}{\partial z}, \tag{20}$$

$$A = \frac{\partial \rho(T,S,p)}{\partial T}\Big|_{S,p}, \tag{21}$$

$$B = \frac{\partial \rho(T,S,p)}{\partial S}\Big|_{T,p}. \tag{22}$$

Consequently, for computing M and N, the vertical gradients of T, S, u and v need to be evaluated at the element interfaces. Here we present two different strategies for obtaining the gradients.

In FE discretisation the most intuitive way to evaluate gradients is by using the gradients of the basis functions. The vertical gradient of a field T is given as $\partial T/\partial z = \sum_{(e,\xi)\in\mathcal{D}} T_{(e,\xi)} \partial \psi_{(e,\xi)}/\partial z$, which is a discontinuous polynomial of degree $o-1$. The nodal values of such a field are given by

$$\left(\frac{\partial T}{\partial z}\right)_{(e,\xi)} = T_{(e,\xi)} \frac{\partial \psi_{(e,\xi)}}{\partial z}\Big|_{\boldsymbol{x}_{(e,\xi)}}, \quad \forall (e,\xi) \in \mathcal{D}.$$

Using the mapping Π_{DG}, an array $(\partial T/\partial z)_{j,i},\ i = 1,\ldots,n_j^{DG}$ is created for each vertical line j, assigning the appropriate values

$$\left(\frac{\partial T}{\partial z}\right)_{j,i} = \Pi_{DG}\left(\frac{\partial T}{\partial z}\right)_{(e,\xi)}. \tag{23}$$

The above values are discontinuous at the element interfaces. An estimate of the gradient can be obtained by taking an arithmetic mean

$$\left(\widehat{\frac{\partial T}{\partial z}}\right)_{j,m} = \frac{1}{2}\left[\left(\frac{\partial T}{\partial z}\right)_{j,2m} + \left(\frac{\partial T}{\partial z}\right)_{j,2m-1}\right], \quad m = 1,\ldots,n_j^{\mathrm{CG}} - 2. \tag{24}$$

The drawback of (24) is that it only uses the gradient in each element, thus ignoring the jump at the interface. The gradient fields also tend to be more noisy than the corresponding scalar fields.

Another possibility is to use finite differencing across the element interface. First, the field nodal values are fetched in the 1D arrays

$$T_{j,i} = \Pi_{\mathrm{DG}} T_{(e,\xi)}. \tag{25}$$

Denoting the z coordinates of each node by $z_{j,i}$, element heights and the total depth are obtained as

$$d_{j,m+1/2} = z_{j,2m+1} - z_{j,2m}, l = 0,\ldots,n_j^{\mathrm{CG}} - 2, \tag{26}$$

$$H_j = z_{j,n_j^{\mathrm{DG}}-1} - z_{j,0}. \tag{27}$$

Next, T is evaluated at element centres using the 1D DG-FE basis functions $\psi_i(\zeta), i = 1,\ldots,n_{1D}^N$, defined on a reference element $\zeta \in [-1,1]$. For first order elements $n_{1D}^N = 2$ and we can write (see Fig. 1):

$$\widetilde{T}_{j,m+1/2} = T_{j,2m}\psi_1(0) + T_{j,2m+1}\psi_2(0), \quad m = 0,\ldots,n_j^{\mathrm{CG}} - 2. \tag{28}$$

For Lagrangian basis functions, we have $\psi_1(0) = \psi_2(0) = 1/2$, implying that the above is equivalent to an arithmetic mean of the nodal values.

Now the vertical gradient of T can be estimated by finite differencing

$$\begin{aligned} &\tilde{d}_{j,m} = \tfrac{1}{2}(d_{j,m+1/2} + d_{j,m-1/2}),\\ &\left(\widehat{\frac{\partial T}{\partial z}}\right)_{j,m} = \frac{\widetilde{T}_{j,m+1/2} - \widetilde{T}_{j,m-1/2}}{\tilde{d}_{j,m}},\\ &m = 1,\ldots,n_j^{\mathrm{CG}} - 2. \end{aligned} \tag{29}$$

The formulation (29) is more accurate because the field values are more reliable at the element centres. Clearly, (29) depends on a stencil of 4 nodal values and thus ignores neither the jump nor the gradient at the interface. To obtain better estimates, more sophisticated interpolation methods could be used, but those are not dealt with in this article.

Once the gradients are obtained, the buoyancy frequency squared is computed as

$$(N^2)_{j,m} = -\frac{g}{\rho_0}\left[A_{j,m}\left(\widehat{\frac{\partial T}{\partial z}}\right)_{j,m} + B_{j,m}\left(\widehat{\frac{\partial S}{\partial z}}\right)_{j,m}\right], \tag{30}$$

where $A_{j,m}$ and $B_{j,m}$ are computed with the mean temperature and salinity at the interface.

The vertical shear frequency is computed in a similar fashion. Denoting the shear frequency in x direction by M_x, the following temporal averages are defined with respect to the velocity field of the previous iteration:

$$(\overline{M}_x)_{j,m} = \delta\left(\widehat{\frac{\partial u}{\partial z}}\right)_{j,m} + (1-\delta)\left(\widehat{\frac{\partial u}{\partial z}}\right)^{\mathrm{old}}_{j,m},$$

$$(\overline{M}'_x)_{j,m} = \frac{1}{2}\left(\widehat{\frac{\partial u}{\partial z}}\right)_{j,m} + \frac{1}{2}\left(\widehat{\frac{\partial u}{\partial z}}\right)^{\mathrm{old}}_{j,m}.$$

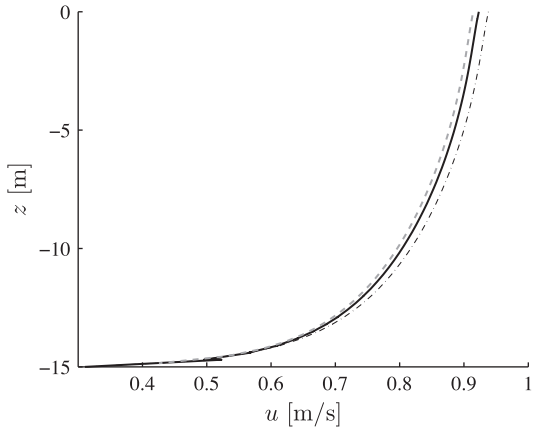

Fig. 2. Steady-state velocity profile for the bottom boundary layer test. Solid line, SLIM + GOTM; Dashed line, GOTM; Dash-dotted line, SLIM + GOTM with FE gradients.

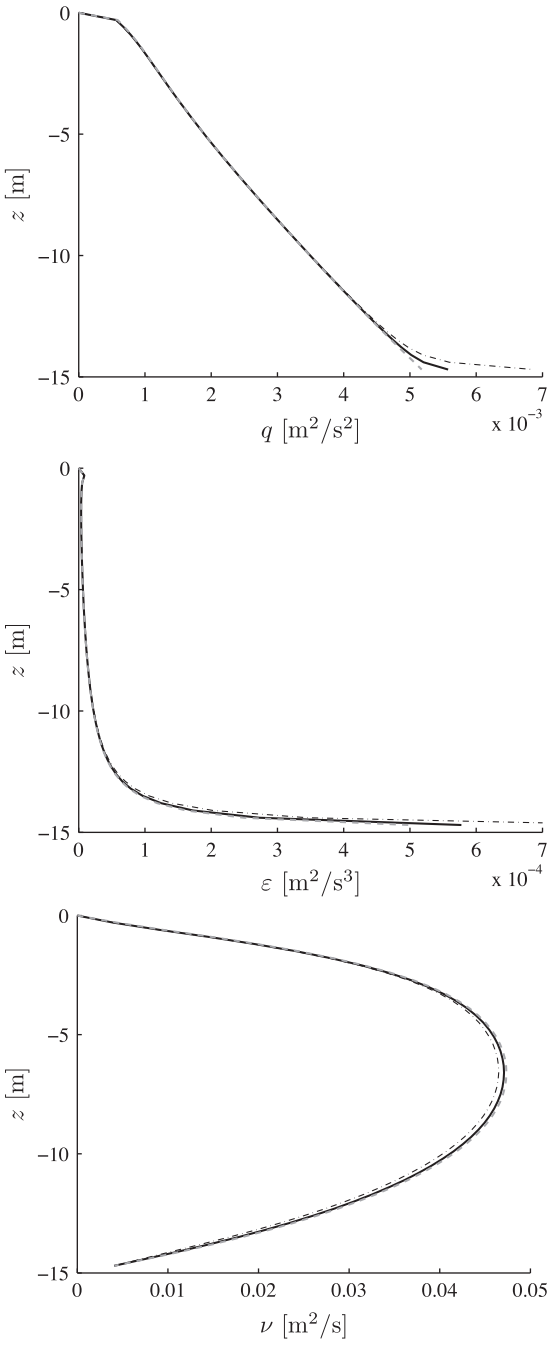

Fig. 3. Profiles of turbulent kinetic energy (top), TKE dissipation rate (middle) and eddy viscosity (bottom). Solid line, SLIM + GOTM; Dashed line, GOTM; Dash-dotted line, SLIM + GOTM with FE gradients.

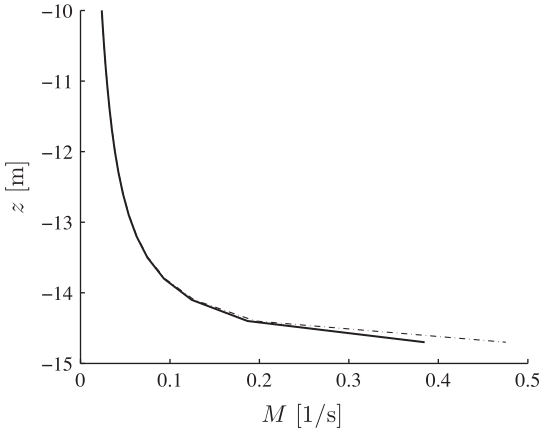

Fig. 4. Vertical shear frequency at the lower part of the water column computed with the FD gradients (solid line) and the FE gradients (dash-dotted line) for the same velocity profile. Here the velocity profile obtained with SLIM + GOTM and FD gradients (solid line in Fig. 2) is used.

The implicity parameter $\delta \in [0,1]$ depends on the temporal scheme of vertical diffusion. Here, the Crank–Nicholson scheme is used for vertical diffusion, so that $\delta = 1/2$.

Now, the square of vertical shear frequency in x direction is:

$$\left(M_x^2\right)_{j,m} = (\overline{M}_x)_{j,m}(\overline{M}'_x)_{j,m}, \quad m = 1,\ldots,n_j^{CG}-2. \tag{31}$$

The shear frequency in y direction, M_y, is computed analogously, with the respective velocity field v. Finally the shear frequency is given by

$$M = \sqrt{M_x^2 + M_y^2}. \tag{32}$$

The temporal averaging in (31), proposed by Burchard (2002), guarantees that the (Reynolds averaged) kinetic energy is transformed to turbulent kinetic energy in a conservative manner, which improves the numerical stability of the TKE computation.

The above formulation for computing N and M is derived for first order Lagrangian DG basis functions, but it similar formulae can be derived for other (e.g. higher order or continuous) function spaces as well.

4.3. Advection of k and Ψ

Eqs. (12) and (16) contain advection terms for k and Ψ, respectively. These terms are not included in the 1D vertical turbulence closure model that deals only with turbulent processes. Therefore k and Ψ are advected in the 3D model as a passive tracer using the same Adams–Bashforth scheme as for T and S.

For stability it is crucial to ensure strict positivity of these variables which may be challenging due to strong gradients. A monotonous tracer advection scheme is achieved by applying a slope limiter similar to that by Aizinger (2011). Slightly negative values (of the order of machine precision) may still appear, which are clipped to a small positive value.

5. Numerical tests

In order to validate the presented coupling, a number of numerical tests were conducted. All the tests were run on SLIM 3D coupled to GOTM. In typical estuarine conditions the k–ε,k–ω and (improved) Mellor–Yamada level 2.5 turbulence closures have proven to produce similar results (e.g. Warner et al., 2005). In these tests a k–ε turbulence closure with the stability functions of Canuto et al. (2001) (Model A) was used. For a detailed set of parameters refer to Burchard et al. (1998).

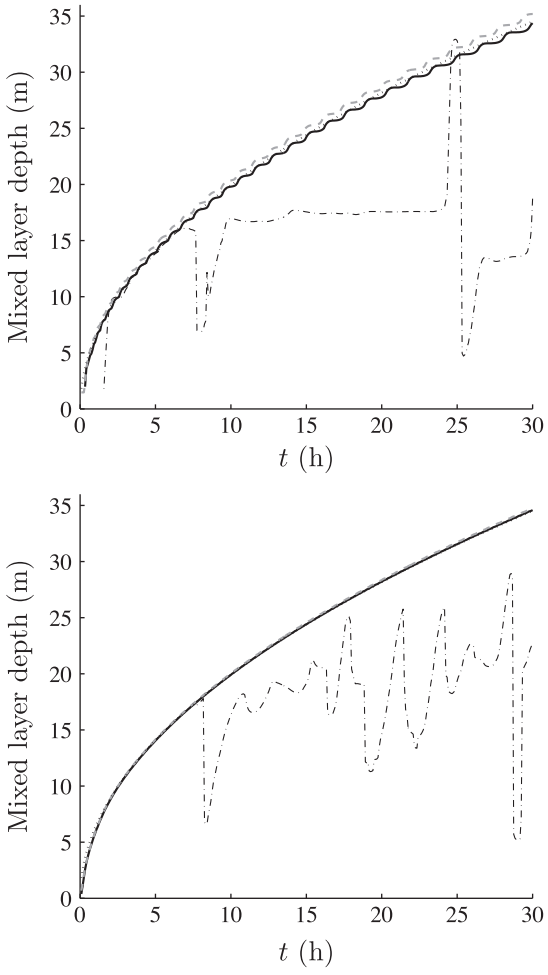

Fig. 5. Mixed layer depth versus time for the Kato–Phillips test with 1 m (top) and 20 cm (bottom) vertical resolution. Solid line, SLIM + GOTM; Dashed line, GOTM. Dotted line, the solution by Price (36); Dash-dotted line, SLIM + GOTM with FE gradients.

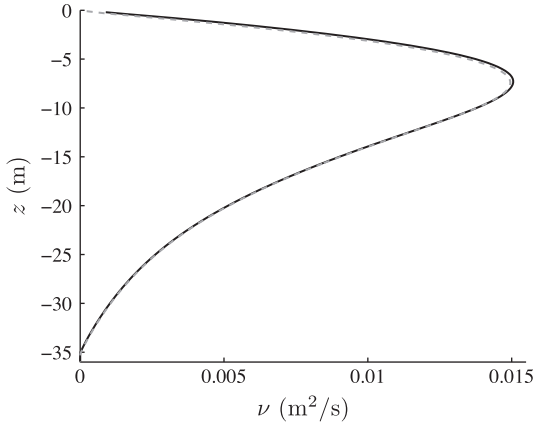

Fig. 6. Turbulent viscosity with 20 cm vertical resolution. Solid line, SLIM + GOTM; Dashed line, GOTM. Results obtained with the FE gradients are omitted.

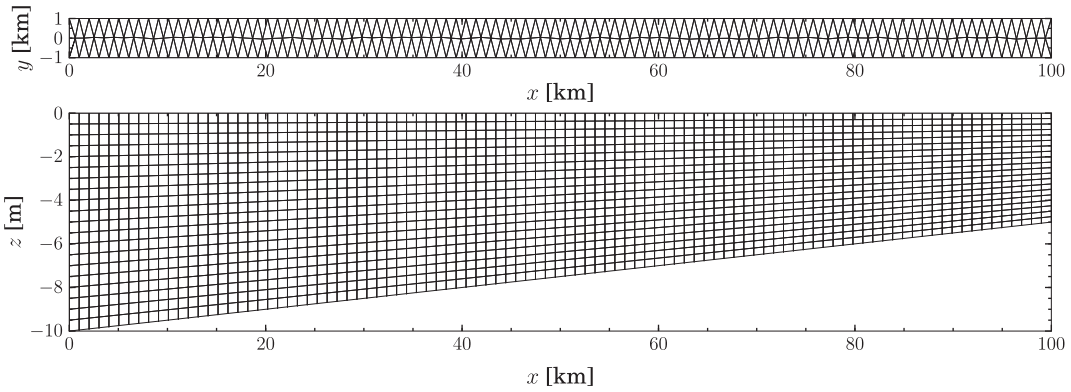

Fig. 7. Estuary simulation: 3D mesh. Horizontal edge length is roughly 1 km. The mesh consist of 396 surface triangles and 7920 prisms.

5.1. Bottom boundary layer

The 3D model's ability to reproduce bottom boundary layer was assessed with pressure gradient driven free flow. The fluid is initially at rest, forced only by a constant free surface slope. In the absence of rotation, the flow velocity near the bottom boundary follows the usual logarithmic profile, which can be expressed as (e.g. Hanert et al., 2007)

$$\boldsymbol{u}(z) = \frac{\boldsymbol{u}_*^b}{\kappa} \log\left(\frac{z_0^b + z + h}{z_0^b}\right), \tag{33}$$

where $\boldsymbol{u}_*^b$ is the bottom friction velocity and κ is the von Karman constant.

In accordance with (33), the conventional quadratic friction law is imposed at the bottom:

$$\nu \frac{\partial \boldsymbol{u}}{\partial z} = c_d |\boldsymbol{u}_b| \boldsymbol{u}_b, \tag{34}$$

$$c_d = \left(\frac{\kappa}{\log\left(\frac{z_b + h + z_0^b}{z_0^b}\right)}\right)^2, \tag{35}$$

where c_d is the drag coefficient, z_b is the vertical coordinate at the middle of the bottom most element and $\boldsymbol{u}_b = \boldsymbol{u}(z_b)$. Using (33) and (35), the bottom friction velocity is obtained as $\boldsymbol{u}_*^b = \sqrt{c_d}\boldsymbol{u}_b$.

Pressure gradient driven free flow was simulated in a 10 km by 10 km square domain in horizontal, 15 m deep, with 30 cm vertical resolution. Throughout the simulation the free surface slope was fixed to -10^{-5} in x direction. Bottom roughness length was $z_0^b = 1.5$ mm. The simulation was run for 24 h until it reached a steady state, i.e. a balance between pressure gradient force and friction. The shear frequency was computed either with finite differencing according to (29) or by the means of the FE basis functions (24). For reference, the same simulation was performed with 1D GOTM alone using its FD mean flow module.[3]

The steady state vertical velocity profile is presented in Fig. 2. SLIM + GOTM produce very similar profile to GOTM when the FD gradients are used. With the FE gradients, on the other hand, the flow velocity is overestimated in the upper part of the water column.

Vertical profiles of turbulent kinetic energy, dissipation rate and turbulent viscosity are presented in Fig. 3. The TKE profile obtained with SLIM + GOTM corresponds very closely to that of GOTM, except at the bottom boundary where TKE is higher. It is seen that he deviation is much larger in the case of FE gradients.

[3] Since the flow is horizontally homogeneous, a 1D vertical model and a 3D model produce comparable results. As a 3D FE model (in contrast to common FD models) cannot be reduced to a 1D vertical model, we are using full SLIM 3D here.

Table 2
Parameters of the estuary simulation. The underscripts R and S stand for river and sea boundary, respectively. $\overline{U}_0$ and $\overline{U}_\tau$ are the depth averaged residual and tidal velocity, respectively, assuming static water depth (h_R and h_S). At the boundaries, $\bar{u}_R$ and $\bar{u}_S$ are prescribed to account for the free surface movement and guarantee constant water volume over a tidal period. Symmetry boundary conditions are used for the three-dimensional velocity. η_R and η_S are taken as the simulated values on the respective boundary.

Parameter	Symbol	Value
Domain dimensions	D_x,D_y	100 km, 2 km
Mesh length scale	L_{xy}	1 km
Vertical layers	n_σ	20
Bathymetry (river)	h_R	5 m
Bathymetry (sea)	h_S	10 m
Salinity (river)	S_R	0 PSU
Salinity (sea)	S_S	30 PSU
Temperature	T_0	10 °C
Tidal period	τ	12 h
Residual velocity	$\overline{U}_0$	-0.08 m s^{-1}
Tidal velocity	$\overline{U}_\tau$	$0.4 \sin\left(\frac{2\pi t}{\tau}\right)$ m s^{-1}
Depth av. velocity	$\bar{u}_R$	$\frac{\overline{U}_0 h_R}{\eta_R + h_R}$ m s^{-1}
Depth av. velocity	$\bar{u}_S$	$\frac{\overline{U}_0 h_S + \overline{U}_\tau h_R}{\eta_S + h_S}$ m s^{-1}
Bottom roughness	z_0^b	0.005 m

Based on these results, the numerical method for computing vertical gradients has a significant impact on the simulated turbulence. Fig. 4 compares the vertical shear frequency M computed with both FD and FE gradients for the same velocity profile. It is seen that FE gradients produce higher M near the bottom, but the difference is confined only to the two bottom most elements. In the central part of the water column, where the velocity profile is smoother, the two methods are in good agreement.

Because $P = \nu M^2$ appears as a source term for both the k and ε equations, overestimation of M explains the high values of TKE and ϵ near the bottom seen in Fig. 3. In the central part of the water column, TKE is almost unaffected, but ε is still slightly overestimated by roughly 1% (not shown), which results in smaller eddy viscosity (bottom panel in Fig. 3), and higher flow velocity (Fig. 2).

Due to the fact that FD gradients also overestimate the bottom TKE slightly, it is plausible that M is somewhat overestimated in this case as well, but resulting difference in the mixing is much smaller.

5.2. Wind-driven entrainment

The next test examines mixed layer deepening due to surface stress, based on the laboratory experiment originally conducted by Kato and Phillips (1969).

Initially the fluid is motionless and linearly stratified. A constant surface stress is applied at the surface. As a consequence, a mixed

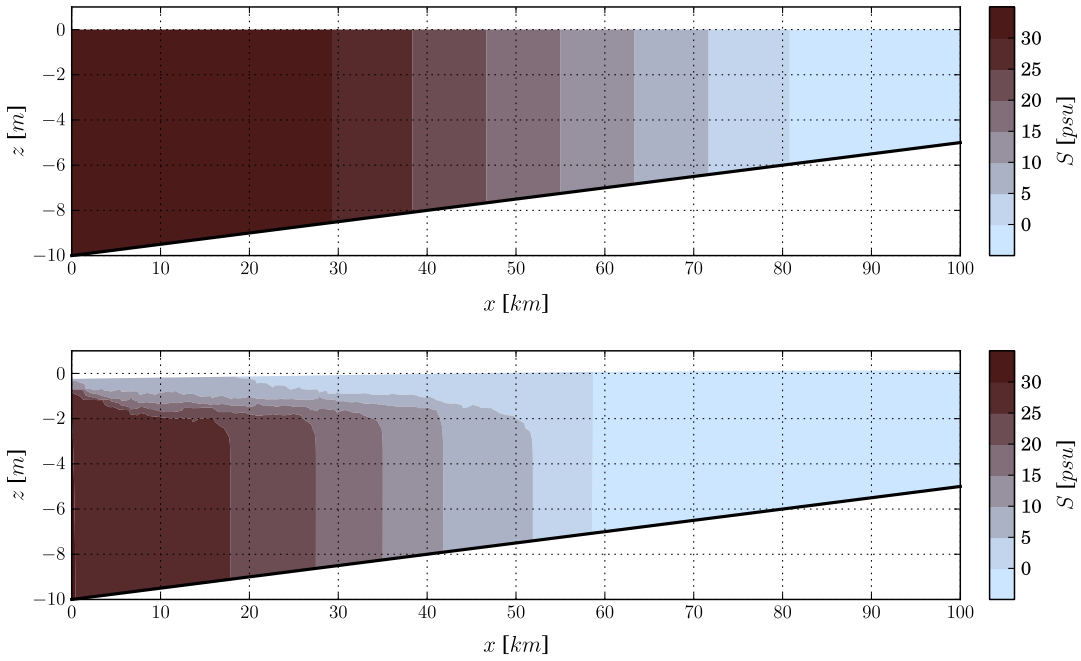

Fig. 8. Estuary simulation: Top: initial salinity distribution. Bottom: salinity after 16 days of simulation.

layer is formed at the surface, growing deeper in time. Price (1979) suggested a formula for the evolution of the mixed layer depth:

$$d_{ML} = 1.05 u_*^s \sqrt{\frac{t}{N_0}}. \tag{36}$$

Here the surface friction velocity is taken as a constant $u_*^s = 0.01$ m s^{-1} while the initial Brunt–Väisälä frequency is $N_0 = 0.01$ s^{-1} following Deleersnijder and Luyten (1994) and Burchard et al. (1998), among others. In practice N_0 is prescribed by imposing a suitable vertical density gradient.

The mixed layer entrainment was simulated in a 50 m deep water column for 30 h. Two vertical resolutions were investigated, namely 1 m and 20 cm. Again, the vertical gradients were computed either with the FD (29) or the FE formulation (24).

Previously it has been concluded that the model's capability to predict the mixed layer deepening depends more on the choice of the stability functions rather that the two-equation model itself (Deleersnijder and Luyten, 1994; Burchard and Deleersnijder, 2001; Umlauf et al., 2003; Deleersnijder et al., 2008). As stated above, we are using the stability functions by Canuto et al. (2001), that have proved out to perform well in this test case.

Evolution of the mixed layer depth, defined as deepest point where $k > 10^{-5}$ m^2 s^{-2}, is shown in Fig. 5 for the two resolutions. The results obtained by SLIM + GOTM (using the FD gradients) are very close to those by GOTM, and both agree well with the formula by Price (36). For a coarser resolution, the mixed layer depth oscillates as mixing penetrates new cells. This is in line with other results, such as in Burchard and Deleersnijder (2001). Turbulent viscosity profile after 30 h of simulation is shown in Fig. 6. The profiles are also very similar, SLIM + GOTM appears to produce marginally larger maximum viscosity.

Using the FE gradients, on the other hand, cause spurious behaviour: the mixed layer depth, defined as the deepest point with significant TKE, oscillates with time. This is due to the fact that the N and M fields are noisy, which occasionally triggers the turbulence model to produce high eddy viscosity at certain nodes, thus mixing the water column in a non-homogeneous manner. Due to these defects, only the more robust FD formulation (29) is considered in the next 3D test case.

5.3. Idealised estuarine circulation

The idealised estuarine scenario proposed by Warner et al. (2005) is used here to verify the behaviour of the turbulence model in a full three-dimensional setting.

The domain is a rectangular basin 100 km long, whose depth varies linearly from 10 m in the "ocean" end ($x = 0$ km) to 5 m in the "river" end ($x = 100$ km). In the cross-channel direction the domain is taken to be 2 km in width with impermeable lateral boundaries. The domain is discretised with 1 km horizontal resolution and 20 sigma layers in the vertical, resulting in 0.25–0.50 m vertical resolution. The mesh is illustrated in Fig. 7 and all the model parameters are presented in Table 2. A constant seaward freshwater discharge is applied at the river boundary, while a sinusoidal tidal flow with 12 h period is prescribed at the ocean boundary. The Coriolis force is neglected. Initially the salinity varies linearly from 30 PSU to 0 PSU between 30 km and 80 km along the channel (Fig. 8). At the ocean boundary the salinity is prescribed to 30 PSU during inflow.

During the simulation, an estuarine circulation quickly develops, driving the saline water under the fresh water. The forming salt wedge oscillates with the tide. The flow stabilises and becomes nearly periodic after roughly 5 days of simulation, when only a small seaward salt flux persists. Warner et al. (2005) designed this test case to compare different turbulence closure models. Indeed, the salinity distribution is largely controlled by vertical mixing, therefore providing a useful benchmark for the SLIM + GOTM coupling.

In this simulation, the 1D turbulence closure models are placed at the centroids of the triangles, as mentioned in Section 4.1. This provides horizontal smoothing of the input fields which improves the stability of the simulation.[4] Similar horizontal filtering is also used in FD models ([e.g.]Burchard and Bolding, 2002). Furthermore, similarly to Warner et al. (2005), the turbulent length scale l is limited from above following Galperin et al. (1988), which also reduces noise in the turbulent quantities.

[4] Note that applying such a filter would have no effect in the two previous test cases where the flow was homogeneous in the horizontal direction.

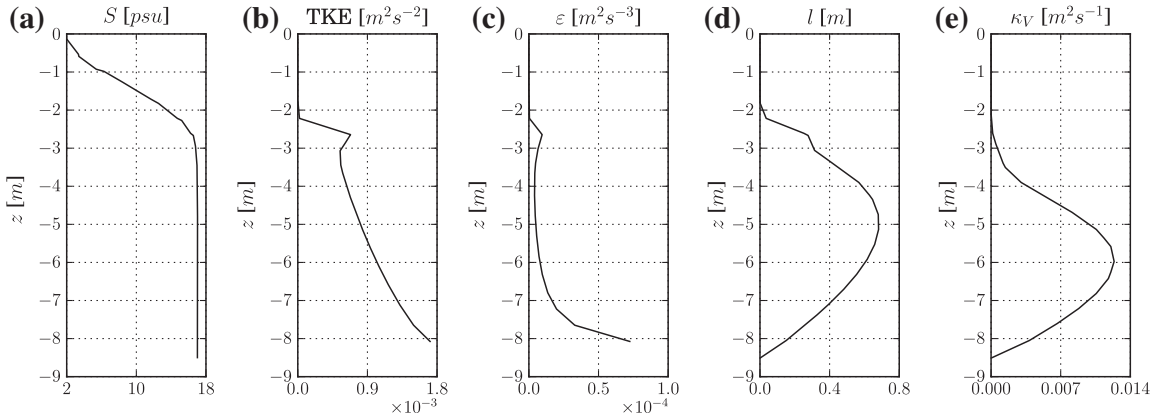

Fig. 9. Estuary simulation: Vertical profiles after 14.40 days of simulation at $x = 30$ km. (a) Salinity, (b) turbulent kinetic energy, (c) TKE dissipation rate, (d) turbulent length scale and (e) eddy diffusivity.

Fig. 8 shows the salt distribution at the end of flood phase, after 16 days of simulation. The salt intrusion is very similar to that obtained with a k–ε model in Warner et al. (2005), where the 0 PSU and 5 PSU contour lines lie between 50 km and 60 km (see Fig. 7 in their manuscript). The surface mixed layer is likewise confined in the first couple of metres of the water column, although it is somewhat thinner than in Warner et al. (2005).

Fig. 9 presents vertical profiles taken at $x = 30$ km after 14.40 days of simulation (corresponding to a typical flood tide). Qualitatively these profiles are similar to those presented in Fig. 9 in Warner et al. (2005). The salinity profile predicted by SLIM + GOTM is identical, but slightly smaller in magnitude (17 PSU versus 20 PSU at the bottom layer). The turbulent length scale is roughly 30% smaller. Turbulent eddy viscosity is also underestimated, the maximum value is 0.013 $m^2\ s^{-1}$ versus nearly 0.02 $m^2\ s^{-1}$. In Warner et al. (2005), the local maximum in TKE is not present for k–ε model, although it appears with other closures.

Taking into account that the turbulent quantities are very sensitive to the characteristics of the flow and details of the turbulence closure, one can conclude that the coupled SLIM + GOTM model produces the expected flow features with good accuracy. In addition to differences in the turbulence closure models, also other aspects, such as the boundary conditions or numerical mixing (Burchard and Rennau, 2008; Rennau and Burchard, 2009) may have a significant impact on the distribution of salinity and turbulent quantities. As Warner et al. (2005) used a structured grid FD model, model-dependent features are likely to play a role. However, assessing such differences is out of the scope of the current article.

6. Conclusions

Implementing turbulence closure models in a discontinuous Galerkin framework is not often addressed in the literature. We have presented an online coupling between a 3D DG-FE marine model and a FD 1D vertical turbulence model, which exploits the vertically orientated topology of the 3D mesh. We demonstrate that such a coupling is not trivial due to the different mesh topology and the discontinuous functional representation of fields.

Ensuring stability of the turbulence closure model is an essential part of the presented methodology. Stability is achieved by suitable data processing, i.e. computing the vertical gradients more reliably at the element interfaces by taking into account all the nodal values in the elements above and below. Further, in horizontal direction the 1D vertical turbulence models are placed at the centre of each column of prisms, which provides horizontal filtering of the input data.

The coupling has been validated with several test cases. Bottom boundary layer is produced accurately, TKE and viscosity profiles are close to those produced by GOTM. The mixed layer deepening in the Kato–Phillips test case is also correctly predicted. Finally the 3D implementation is validated in an idealised estuary simulation where the results are well in line with those presented in Warner et al. (2005).

In the future the coupled model will be applied to more complicated benchmarks and real world applications.

Acknowledgements

Tuomas Kärnä is a Research fellow with the Belgian Fund for Research in Industry and Agriculture (FRIA). Eric Deleersnijder is an honorary Research associate with the Belgian National Fund for Scientific Research (FNRS). The present study was carried out in the framework of the project "Taking up the challenges of multi-scale marine modelling", which is funded by the Communauté Française de Belgique under contract ARC 10/15-028 (Actions de recherche concertes) with the aim of developing and using SLIM (www.climate.be/slim) and the projectTracing and Integrated Modelling of Natural and Anthropogenic Effects on Hydrosystems (TIMOTHY), an Interuniversity Attraction Pole (IAP6.13) funded by the Belgian Federal Science Policy Office (BELSPO).

References

Aizinger, V., 2011. A geometry independent slope limiter for the discontinuous galerkin method. In: Computational Science and High Performance Computing IV. In: Krause, E., Shokin, Y., Resch, M., Kröner, D., Shokina, N. (Eds.), . Notes on Numerical Fluid Mechanics and Multidisciplinary Design, Vol. 115. Springer, Berlin/ Heidelberg, pp. 207–217.

Blaise, S., Comblen, R., Legat, V., Remacle, J.F., Deleersnijder, E., Lambrechts, J., 2010. A discontinuous finite element baroclinic marine model on unstructured prismatic meshes. Part I: Space discretization. Ocean Dynamics 60, 1371–1393.

Blaise, S., Deleersnijder, E., 2008. Improving the parameterisation of horizontal density gradient in one-dimensional water column models for estuarine circulation. Ocean Science 4, 239–246.

Blaise, S., Deleersnijder, E., White, L., Remacle, J.F., 2007. Influence of the turbulence closure scheme on the finite-element simulation of the upwelling in the wake of a shallow-water island. Continental Shelf Research 27, 2329–2345.

de Brye, B., de Brauwere, A., Gourgue, O., Kärnä, T., Lambrechts, J., Comblen, R., Deleersnijder, E., 2010. A finite-element, multi-scale model of the Scheldt tributaries, river, estuary and ROFI. Coastal Engineering 57, 850–863.

Burchard, H., 2002. Applied turbulence modelling in marine waters. Lecture Notes in Earth Sciences, Vol. 100. Springer, Berlin.

Burchard, H., Baumert, H., 1995. On the performance of a mixed-layer model based on the k–ε turbulence closure. Journal of Geophysical Research 100, 8523–8540.

Burchard, H., Bolding, K., 2002. GETM – a general estuarine transport model. Scientific Documentation. Technical Report EUR 20253 EN, European Commission.

Burchard, H., Bolding, K., Villarreal, M.R., 1999. GOTM, a general ocean turbulence model. Theory, implementation and test cases. Technical Report EUR 18745, European Commission.

Burchard, H., Deleersnijder, E., 2001. Stability of algebraic non-equilibrium second-order closure models. Ocean Modelling 3, 33–50.

Burchard, H., Hetland, R.D., 2010. Quantifying the contributions of tidal straining and gravitational circulation to residual circulation in periodically stratified tidal estuaries. Journal of Physical Oceanography 40, 1243–1262.

Burchard, H., Petersen, O., Rippeth, T.P., 1998. Comparing the performance of the Mellor–Yamada and the k–ϵ two-equation turbulence models. Journal of Geophysical Research 103, 10543–10554.

Burchard, H., Rennau, H., 2008. Comparative quantification of physically and numerically induced mixing in ocean models. Ocean Modelling 20, 293–311.

Canuto, V.M., Howard, A., Cheng, Y., Dubovikov, M.S., 2001. Ocean turbulence. Part I: One-point closure model – momentum and heat vertical diffusivities. Journal of Physical Oceanography 31, 1413–1426.

Chen, C., Beardsley, R.C., Cowles, G., 2006. An unstructured grid, finite-volume coastal ocean model: FVCOM user manual. Technical Report 06-0602, SMAST/UMASSD.

Cheng, Y., Canuto, V.M., Howard, A.M., 2002. An improved model for the turbulent PBL. Journal of the Atmospheric Sciences 59, 1550–1565.

Comblen, R., Blaise, S., Legat, V., Remacle, J.F., Deleersnijder, E., Lambrechts, J., 2010. A discontinuous finite element baroclinic marine model on unstructured prismatic meshes. Part II: Implicit/explicit time discretization. Ocean Dynamics 60, 1395–1414.

Deleersnijder, E., Hanert, E., Burchard, H., Dijkstra, H., 2008. On the mathematical stability of stratified flow models with local turbulence closure schemes. Ocean Dynamics 58, 237–246.

Deleersnijder, E., Luyten, P., 1994. On the practical advantages of the quasi-equilibrium version of the Mellor and Yamada level 2.5 turbulence closure applied to marine modelling. Applied Mathematical Modelling 18, 281–287.

Enstad, L.I., Rygg, K., Haugan, P.M., Alendal, G., 2008. Dissolution of a CO_2 lake, modeled by using an advanced vertical turbulence mixing scheme. International Journal of Greenhouse Gas Control 2, 511–519.

Galperin, B., Kantha, L.H., Hassid, S., Rosati, A., 1988. A quasi-equilibrium turbulent energy model for geophysical flows. Journal of the Atmospheric Sciences 45, 55–62.

Griffies, S.M., 2010. Elements of MOM4p1. Technical Report No. 6, NOAA/Geophysical Fluid Dynamics Laboratory, GFDL Ocean Group.

Hanert, E., Deleersnijder, E., Blaise, S., Remacle, J.F., 2007. Capturing the bottom boundary layer in finite element ocean models. Ocean Modelling 17, 153–162.

Hanert, E., Deleersnijder, E., Legat, V., 2006. An adaptive finite element water column model using the Mellor–Yamada level 2.5 turbulence closure scheme. Ocean Modelling 12, 205–223.

Holt, J., Umlauf, L., 2008. Modelling the tidal mixing fronts and seasonal stratification of the Northwest European Continental shelf. Continental Shelf Research 28, 887–903.

Jackett, D.R., McDougall, T.J., Feistel, R., Wright, D.G., Griffies, S.M., 2006. Algorithms for density, potential temperature, conservative temperature, and the freezing temperature of seawater. Journal of Atmospheric and Oceanic Technology 23, 1709–1728.

Kato, H., Phillips, O.M., 1969. On the penetration of a turbulent layer into stratified fluid. Journal of Fluid Mechanics 37, 643–655.

Lambrechts, J., Comblen, R., Legat, V., Geuzaine, C., Remacle, J.F., 2008. Multiscale mesh generation on the sphere. Ocean Dynamics 58, 461–473.

Luyten, P.J., Deleersnijder, E., Ozer, J., Ruddick, K.G., 1996. Presentation of a family of turbulence closure models for stratified shallow water flows and preliminary application to the Rhine outflow region. Continental Shelf Research 16, 101–130.

Mellor, G., Yamada, T., 1982. Development of a turbulence closure model for geophysical fluid problems. Reviews of Geophysics & Space Physics 20, 851–875.

Osborn, T.R., 1980. Estimates of the local rate of vertical diffusion from dissipation measurements. Journal of Physical Oceanography 10, 83–89.

Pacanowski, R.C., Philander, S.G.H., 1981. Parameterization of vertical mixing in numerical models of tropical oceans. Journal of Physical Oceanography 11, 1443–1451.

Price, J.F., 1979. On the scaling of stress-driven entrainment experiments. Journal of Fluid Mechanics 90, 509–529.

Rennau, H., Burchard, H., 2009. Quantitative analysis of numerically induced mixing in a coastal model application. Ocean Dynamics 59, 671–687.

Rodi, W., 1987. Examples of calculation methods for flow and mixing in stratified flows. Journal of Geophysical Research 92, 5305–5328.

Ruddick, K., Deleersnijder, E., Luyten, P., Ozer, J., 1995. Haline stratification in the Rhine-Meuse freshwater plume: a three-dimensional model sensitivity analysis. Continental Shelf Research 15, 1597–1630.

Rygg, K., Enstad, L., Alendal, G., 2009. Simulating CO2 transport into the ocean from a CO_2 lake at the seafloor using a z- and a σ-coordinate model. Ocean Dynamics 59, 795–808.

Shih, L.H., Koseff, J.R., Ferziger, J.H., Rehmann, C.R., 2000. Scaling and parameterisation of stratified homogeneous turbulent shear flow. Journal of Fluid Mechanics 412, 1–20.

Tian, R., Chen, C., 2006. Influence of model geometrical fitting and turbulence parameterization on phytoplankton simulation in the Gulf of Maine. Deep Sea Research Part II: Topical Studies in Oceanography 53, 2808–2832.

Umlauf, L., Burchard, H., 2003. A generic length-scale equation for geophysical turbulence models. Journal of Marine Research 235–265 (31).

Umlauf, L., Burchard, H., 2005. Second-order turbulence closure models for geophysical boundary layers. A review of recent work. Continental Shelf Research 25, 795–827.

Umlauf, L., Burchard, H., Hutter, K., 2003. Extending the k–[omega] turbulence model towards oceanic applications. Ocean Modelling 5, 195–218.

Wang, Q., 2007. The finite element ocean model and its aspect of vertical discretization. Ph.D. thesis. Universität Bremen.

Warner, J.C., Sherwood, C.R., Arango, H.G., Signell, R.P., 2005. Performance of four turbulence closure models implemented using a generic length scale method. Ocean Modelling 8, 81–113.

White, L., Deleersnijder, E., Legat, V., 2008. A three-dimensional unstructured mesh finite element shallow-water model, with application to the flows around an island and in a wind-driven, elongated basin. Ocean Modelling 22, 26–47.

Wijesekera, H.W., Allen, J.S., Newberger, P.A., 2003. Modeling study of turbulent mixing over the continental shelf: comparison of turbulent closure schemes. Journal of Geophysical Research 108, 3103.

Wilcox, D.C., 1988. Reassessment of the scale-determining equation for advanced turbulence models. AIAA Journal 26, 1299–1310.

Zhang, Y., Baptista, A.M., 2008. SELFE: a semi-implicit Eulerian–Lagrangian finite-element model for cross-scale ocean circulation. Ocean Modelling 21, 71–96.